Developing Damage Assessment Model for Bridge Surroundings: A Study of Disaster by Typhoon Morakot in Taiwan

Jieh-Haur Chen and Pei-Fen Huang

Abstract—This paper presents an integrated model that automatically measures the change of rivers, damage area of bridge surroundings, and change of vegetation. The proposed model is on the basis of a neurofuzzy mechanism enhanced by SOM optimization algorithm, and also includes three functions to deal with river imagery. High resolution imagery from FORMOSAT-2 satellite taken before and after the invasion period is adopted. By randomly selecting a bridge out of 129 destroyed bridges, the recognition results show that the average width has increased 66%. The ruined segment of the bridge is located exactly at the most scour region. The vegetation coverage has also reduced to nearly 90% of the original. The results yielded from the proposed model demonstrate a pinpoint accuracy rate at 99.94%. This study brings up a successful tool not only for large-scale damage assessment but for precise measurement to disasters.

Keywords—remote sensing image, damage assessment, typhoon disaster, bridge, ANN, fuzzy, SOM, optimization.

I. INTRODUCTION

TAIWAN is an eco-rich island but severe stricken by natural forces every year. Among nature strikes to Taiwan, the earthquake and typhoon are the majority, resulting in severe damage to residents and economic activities. Catastrophic earthquake may claim hundreds of lives and billions of economic losses such as Chi-chi earthquake in 2001. Fortunately, the frequency of such quake occurring in Taiwan is relatively low, that is, once in decades. On the other hand, disasters caused by typhoon strikes are much more devastated. There are 383 typhoons directly striking the Taiwan Island in the past century, excluding those which passed by but still claimed loss of lives and economic activities. The average annual loss due to typhoon strikes reaches approximately $1 billion US dollars [1]. Losses due to typhoon invasions have always been one of major issues to the Taiwan society. Among them, destruction of bridges can easily bring in such enormous losses.The bridge is one of important infrastructures connecting social groups and economic activities.

Jieh-Haur Chen is with the Institute of Construction Engineering and Management, National Central University, Jhongli, Taoyuan 32001, Taiwan. (phone: +886-3-4227151 ext. 34112; fax: +886-3-4257092; e-mail: jhchen@ncu.edu.tw).

Pei-Fen Huang is with the Institute of Construction Engineering and Management, National Central University, Jhongli, Taoyuan 32001, Taiwan. (phone: +886-3-4227151 ext. 34036; fax: +886-3-4257092; e-mail: pavanhuang@gmail.com).

Brides usually have long period of useful lives and are designed to stand for intensive use. They do not deteriorate sharply unless destructive power comes. Destructive power such as floods brought by tremendous precipitation of typhoon can easily exceed bridge limits. Bridges usually stand no chance to resist such awesome power of nature. For example, the Typhoon Morakot ruined a total of 129 bridges, which is the record high number of destroyed bridges by a single cause of the nature force. To assure safety and to pursue better site selection for rebuilt structures, the surroundings of damaged bridges that may cause potential secondary influence to occupants and structure should be measured and estimated. The research objectives are to present an integrated model that automatically measures the change of rivers, damage area of bridge surroundings, and change of vegetation and, then to provide site-selecting information for bridge reconstruction. The scope limits to the suppositions of the acquisition of remote sensing images from a single satellite (FORMOSAT-2), the use of remote sensing RGB images that have already been calibrated and fine-tuned, and manual recognition by experts and field observations that are involved as the final validation for pattern classification.

II. APPLICATIONS AND ALGORITHMS FOR DAMAGE ASSESSMENT

Applications and algorithms utilized for damage assessment are numerous. Studies adopted various types of images to deal with damage assessment. These include, for example, ultrasound spectroscopy, laser imagery, remote sensing image, synthetic aperture radar image, and thermal image [2]-[6]. For large scale damage assessment, analysis or assessment based on remote sensing imagery is the majority. Scholars developed a rapid damage assessment of built-up structures. Applications can be found in its succeeding studies[7],[8]. The concept of earthquake damage map based on analysis of remote sensing images has brought attention to rescuers[9]. A preparation map for earthquake damage assessment was proposed to assist rescuers in outlining rescue plans [10]. Large scale disasters also occur as tsunami invades. Scholars integrated remote sensing imagery with GIS techniques to facilitate damage assessment for the tsunami invasion in the southern Asia, 2004 [11]. Other studies pointed out the benefits of using remote sensing images to estimate tsunami impact [12]-[16] Destruction brought by typhoons as well as that of above-mentioned nature calamities usually covers sizable area. Related work showed that remote sensing is an effective

technique to determine quantities of damage areas[17],[18]. Vegetation damage can be measured using remote sensing analysis. Estimating crop damage traditionally follows the technique of field observations, which results in a time-consuming task. An attempt to exploit remote sensing images imparted promising feasibility[19]. Another related study identifying cotton injury through the use of remote sensing images seconded that multispectral imaging is a viable tool[20]. Forest management is one of research fields that frequently require remote sensing techniques to deal with recognition. Such studies can be found in wood resource investigation, forest fire, carbon emissions, forest damage, and so on[21],[22],[18],[23]. An investigation presented a high accuracy rate of image-based damage assessment, compared to field inventory estimates. It suggested that the satellite image-based assessment should not require pre-disturbance field inventory data. The use of remote sensing image has no doubt in saving efforts and providing high accuracy for large-scale damage assessment.Past studies have introduced various techniques that are capable of handling different demands of image recognition. Over two decades ago, scientists started to track contamination for forest using remote sensing techniques[24]. Bernstein and Di Gesù in 1999 developed an object recognition system to extract shape information from remote sensing images. The unsupervised change-detection methods achieved a better estimate of the optimal threshold value[25]. A clustering technique was adopted to detect deterioration of structures for damage assessment[26]. Wang et al. performed a comparison among four algorithms employed to detect forest change due to hurricane invasion. These algorithms were univariate image differencing (UID), selective principal component analysis (PCA), change vector analysis (CVA), and post-classification comparison (PCC). The last one along with the composite image yielded the best results but all four algorithms are still subject to some restrictions[27]. A probabilistic classification framework was developed to provide posterior probabilities for regional urban. The approach classified damage levels that deterministic approaches would not solve[28]. With remote sensing information, techniques adopted to measure the change of rivers are rare but can be found such as k nearest neighbor (KNN), objective-oriented supervised classification, raster-based classification [29],[30]. However, they claimed that the methods would not resolve river damage by floods. A novel technique is imperative to overcome the aforementioned shortcoming.

III. ACQUISITION AND ANALYSIS OF REMOTE SENSING IMAGES

All remote sensing images for this research are acquired based on geometry-calibrated imagery of FORMOSAT-2 satellite. The FORMOSAT-2 imagery is a high resolution image with characteristics of: (1) multispectral resolution of 8m, (2) RGB wavelength from 0.45 to 0.69 μm, and (3) image swath of 24km with limb view angle ±45°. The geometric calibration for the images is carried out to eliminate spatial errors as precision ground control points and digital terrain model are available. However, most acquired images are regarding those distroyed bridges and their surroundings located in mountain or remote districts. It is difficult to have

precision ground control points and digital terrain model ready for the calibration. To eliminate these errors, we apply linear deformation as an affine transformation plus manually digitized image control points [31].There are 129 bridges being destroyed during the Typhoon Morakot invasion in the August of 2009. Over a half of which are located in remote districts and serve for relatively less population. The priority to recover damaged bridges is mainly on the basis of bridge service capacity, that is, population. The selection of destroyed bridges follows such demand and, thus, considers those located in the midstream or downstream of rivers. Randomly choosing one out of the total 36 destroyed bridges located in the midstream or downstream of rivers, we present the FORMOSAT-2 satellite images (Figure 1) taken 10 days before and after the typhoon strike, respectively. The circled part in Figure 2 shows the ruined segment of the bridge. In the left hand side of Figure 1, there is nearly no landslide occurring in the river headstream. It is also clear that the bridge is not located in the scour side of the river. The record-high amount of precipitation did cause significant change of the river shown in Figure 2. The rectangular highlights a smashed segment of embankment by serious scour during the floods.

Fig.1 Baolai-2 Bridge and its surroundings before and after Typhoon Morakot strike

Fig.2 Distroyed bridge segment and flooded area

IV. DEVELOPMENT OF RECOGNITION MODEL

The proposed model is founded on the work by Su et al. in 2011; yet, it is modified with fuzzy and optimization algorithms so as to handle imagery of the flooded areas that particularly mixes with the river courses and landslide areas. Given a typical artificial neural network, to make sure a full training, the supervised decision directed learning algorithm is used:

$$Out(x) = f\left(\sum_{j=1}^{J} Out_j(x) - \eta\right), \quad (1)$$

$$Out_j(\underline{x}) = f\left(net_j(x)\right), \quad (2)$$

$$net_j(\underline{x}) = \sum_{i=1}^{p} f\left((M_{ji} - x_i)(x_i - m_{ji})\right) - p , \quad (3)$$

$$f(x) = \begin{cases} 1 & if \quad x \geq 0 \\ 0 & if \quad x < 0 \end{cases}, \quad (4)$$

where M_{ji} and $m_{ij} \in R$ are the weights of the jth neuron of the hidden layer, $\underline{x} = (x_1, ..., x_p)^T$ stands for training data, p is the dimension of the input variable, $\eta \in R$, and the output is $Out(\underline{x})$: $R^p \rightarrow \{0,1\}$. To overcome possible difficulty of recognizing hazy areas, the neural network needs to embrace the fuzzy approach. Therefore, $m_j(\underline{x})$ is employed to replace (4) as follows:

$$m_j(\underline{x}) = \exp\left\{-s_j^2\left[per_j(\underline{x}) - per_j\right]^2\right\} . \quad (5)$$

$$where \quad per_j = \sum_{i=1}^{p}\left(M_{ji} - m_{ji}\right); \quad (6)$$

$$per_j(\underline{x}) = \sum_{i=1}^{p} \max\left(M_{ji} - m_{ji}, x_i - m_{ji}, M_{ji} - x_i\right). \quad (7)$$

The output, accordingly, is re-written as:

$$Out(\underline{x}) = \sum_{j=1}^{J} w_j m_j(\underline{x}) + \theta , \quad (8)$$

where w_j is the weight of the jth neuron of the hidden layer, s_j is the sensitivity, and θ indicates an adjustable value. At this stage the proposed model is ready for pattern recognition; nevertheless, the parameter settings may fail to reach optimization so that the accuracy rate of recognition cannot be optimal. Since the practicability of the self-organizing map optimization (SOMO) algorithm in dealing with optimization problems has been demonstrated [32]-[34], let each parameter set of the network have a corresponding vector in $[l_1,h_1] \times ... \times [l_n,h_n]$. After initializing, the winner neuron j^* can be expressed by:

$$j^* = Arg \max_{1 \leq j \leq M \times N} \varphi_j(\underline{x}(k), \underline{w}_j(k))$$
$$= Arg \min_{1 \leq j \leq M \times N} \|\underline{x}(k) - \underline{w}_j(k)\| , \quad (9)$$

where $\underline{x}(k)$ is an input pattern; $\underline{x}(k) = [x_1(k),...,x_n(k)]^T$ represents the kth input pattern; $\varphi_j(\cdot,\cdot)$ is for the activation function of neuron j; and $\|\cdot\|$ is the Euclidean norm. To assure optimization for settings, we need to fine-tune the weighs of j* and its neighbors using:

$$\underline{w}_j(k+1) = \underline{w}_j(k) + \lambda_1 \Lambda_{j^*,j}[\underline{w}_{j^*}(k) - \underline{w}_j(k)]$$
$$+ \lambda_2(1 - \Lambda_{j^*,j})\underline{n} , \quad (10)$$
$$for \quad 1 \leq j \leq M \times N$$

where $\Lambda_{j^*,j} = 1 - \dfrac{d_{j^*,j}}{\sqrt{M^2 + N^2}}$; λ_1 and λ_2 are the learning rates, usually in the ranges of $0 < \lambda_1 \leq 0.3$ and $0 < \lambda_2 \leq 0.2$; $\underline{n} = (n_1, \cdots, n_n)^T$ is defined as a noise vector for the new weight vector. Next the proposed approach is applied to the imagery provided by FORMOSAT-2 which belongs to the RGB image type. Figure 3 shows the pre-selected training fields. Starting with the threshold settings of RGB pixels from 0 to 255, we determine the settings for forest, for instance, by the following expression:

$$I'(x,y) = \begin{cases} I(x,y), & if \ 140 \leq B_{xy} \leq 255 \\ & and \ if \ 50 \leq R_{xy} \leq 255 \\ 0, & else \end{cases} \quad (11)$$

where $I'(x,y)$ is the labeled RGB value of the pixel I at (x,y) coordination, $I(x,y)$ is the original RGB value for the pixel I, and B_{xy} and R_{xy} represent the blue and red values of the pixel I. Figure 4 illustrates the result for labeled forest in black color. Comparing these two images, we are able to obtain the assessment of damaged forest area. The illustration of Figure 5 demonstrates how the comparison works. Similarly the built-up area can be also estimated following the process.
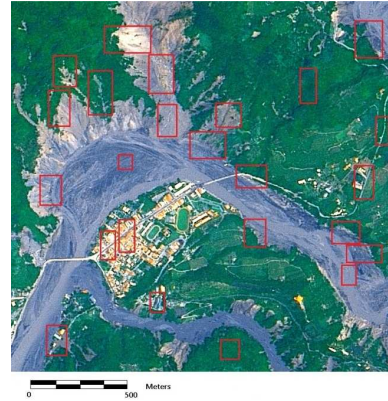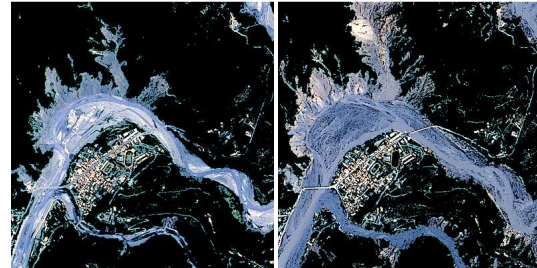

Fig. 3 Pre-selected training fields

Fig. 4 Labeled forest area before and after the typhoon invasion

P_{i1j1} (25)	P_{i2j1} (3)	P_{i3j1} (31)		P_{i1j1} (20)	P_{i2j1} (35)	P_{i3j1} (30)		P_{i1j1} (5)	P_{i2j1} (-5)	P_{i3j1} (1)
P_{i1j2} (13)	P_{cente} (6)	P_{i3j2} (65)	−	P_{i1j2} (13)	P_{center} (15)	P_{i3j2} (15)	=	P_{i1j2} (0)	P_{center} (50)	P_{i3j2} (5)
P_{i1j3}	P_{i2j3}	P_{i3j3}		P_{i1j3}	P_{i2j3}	P_{i3j3}		P_{i1j3}	P_{i2j3}	P_{i3j3}

(3)	(8)	(68)

(3)	(66)	(72)

(0)	(23)	(-4)

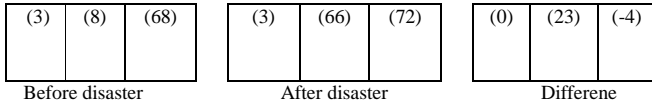Before disaster   After disaster   Differene

Fig. 5 Illustration for comparison of before and after disaster images

For river image recognition, there are additional two steps — dilation and erosion — to compute change of rivers. The dilation step is to find any pixel in the river with its $I' = 0$ and then to identify its neighbors' I' values in a smallest area (3 by 3). Once any neighbor with $I' \neq 0$ is spotted, the proposed model resets its value to 0. Through certain iterations determined by a pre-specified number or no more pixel $I' \neq 0$ found, the dilation stops and the next step of erosion kicks in. The erosion step is similar to a reversed process of the dilation step so as to restore the original river pixels without noise. In this step the proposed model seeks those pixels being "dilated" in the last step. Finding a "dilated" pixel with $I' \neq 0$, the proposed model sets all $I' = 1$ when spotting any $I' = 0$ in the smallest neighbor area. This step repeats till the pre-specified number of iteration is reached or no more pixel $I' = 0$ found. Up to now, the river width can be calculated. The proposed model also measures change of rivers. Heavy precipitation may trigger landslide and floods presenting similar imagery, which cause difficulty for recognition. The additional function of skeletonization provided by the proposal model outlines the main river course, detects new stream courses, and differentiates flooded or landslide area. These tasks can be done through the determination of river "skeleton". Assuming that in an M by N neighbor pixel area, we define $N(P) = \sum_{i=1; j=1}^{i=M; j=N} p_{ij}$ (1) and $S(P) = \sum_{i=1; j=1}^{i=M; j=N} p_{ij}$ (0) illustrated in Figure 6. To facilitate computation, M and N are usually set to a smallest neighbor area (3 by 3). All pixels in the area are removed if satisfying:

$$if \begin{pmatrix} 2 \leq N(P) \leq 6; S(P)=1; P_{i2j1} \cdot P_{i3j2} \cdot P_{i2j3}=0; P_{i3j2} \cdot P_{i2j3} \cdot P_{i1j2}=0 \\ 2 \leq N(P) \leq 6; S(P)=1; P_{i2j1} \cdot P_{i3j2} \cdot P_{i1j2}=0; P_{i2j1} \cdot P_{i2j3} \cdot P_{i1j2}=0 \end{pmatrix} (12)$$

Then all pixels are removed.

However, no pixel is removed when satisfying $N(P) = 0$, $N(P) = 1$, $N(P) > 6$, or $S(P) = 0$ where the pixel represents the edge point. The establishment for the proposed model is complete and Figure 7 demonstrates the model interface by using C++ language.

■	□	□
■	■	■
■	■	■

→

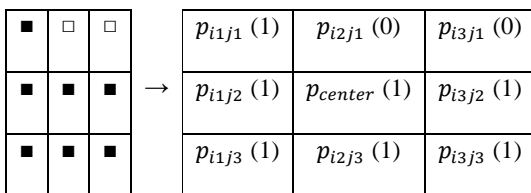| p_{i1j1} (1)	p_{i2j1} (0)	p_{i3j1} (0)
p_{i1j2} (1)	p_{center} (1)	p_{i3j2} (1)
p_{i1j3} (1)	p_{i2j3} (1)	p_{i3j3} (1)

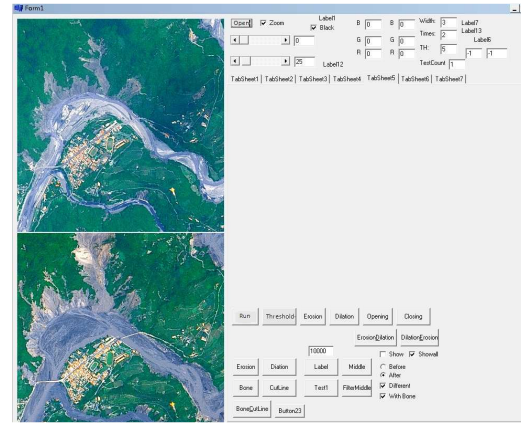Fig. 6 Illustration for river skeletonization

Fig. 7 Model interface

V. IMPLEMENTATION AND DISCUSSION

After opening the before- and after-disaster images, we can measure the change of landslide, river width, flooded area, and vegetation coverage. The model is designed to yield results automatically or semi-automatically. Since RGB values are all set based on the default ranges, i.e. in Equation (11), the model performs automatically and discovers that the vegetation coverage has reduced to 89.95% of the original because of the typhoon invasion. The loss of most vegetation is due to massive landslide beside the river and its branches. For the river increment, Figure 8 illustrates the results yielded from the proposed model. It is found that the ruined bridge segment is precisely located at one of scour sites during the typhoon invasion. Structure reinforcement or relocation for the bridge is strongly suggested. With the use of the dilation, erosion, and skeletonization functions, the changed river courses due to the typhoon strike can be distinguished in Figure 9.

The proposed model also measures that the average river width has increased to 1.67 times of the original. Figure 10 indicates a comparison for the change of river width. According to field observations, the original length of Baolai-2 Bridge and the shore-to-shore width were 158 and 160 meters, respectively. Observations conducted after the invasion reports that the shore-to-shore width of the river at the bridge location has increased to 195.44 meters [35]. The result yielded from the proposed model presents a pinpoint accuracy rate at 99.94%. The proposed model presents a successful tool not only for large-scale damage assessment but for precise measurement to disasters.
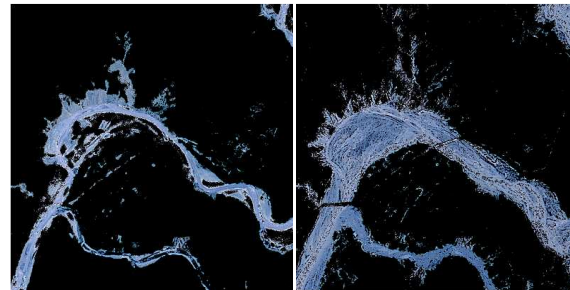
Before typhoon invasion   After typhoon invasion
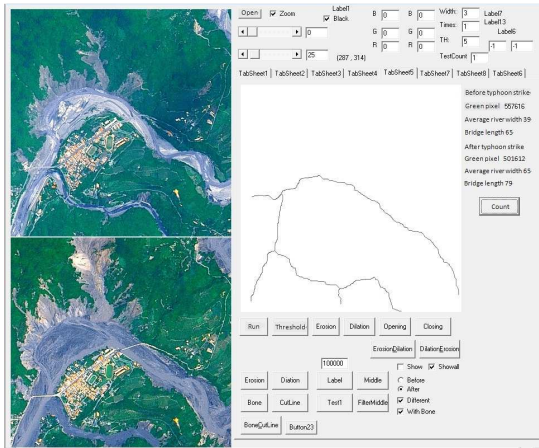
Fig. 8 Change of river course

Fig. 9 River skeleton and results

Fig. 10 Comparison of river change

VI. CONCLUSION

This paper develops a model to estimate post-typhoon damage around ruined bridges based on remote sensing imagery. The proposed model is designed to integrate computational intelligence with image process techniques and, therefore, provides quick and precise measurement for the change of vegetation, landslide, built-up area, river course, river width, and scouring site. By outlining the river skeleton and revealing the river courses, it is found that the broken segment is located exactly at one of the scour sides of the river. The pinpoint accuracy is also demonstrated in the example of measuring the river shore-to-shore width. Such information is critical for bridge rehabilitation or even site selection for bridge renewal. As a result, the major contributions can be summarized as (1) a novel technique that effectively deals with large-scale assessment at high accuracy, (2) determination of key information for bridge rehabilitation or renewal, and (3) notation for follow-up monitoring.

Further utilizing the results from this research, the succeeding studies could gain more valuable information in practice. Examples can be expected in instant responses to rescue mission, hazard management, and management of natural recourses. The results may play a crucial role especially for those disasters occurring in inaccessible zones. Another potential follow-up studies would focus on detailed recognition of how bridges deteriorate due to river scour. Further analysis considering bridge deterioration and river courses may bring up comprehensive suggestions for building design and planning. A close-up detection for bridge themselves may be developed to identify possible damage that could take place during next severe strikes by nature force. Integrated with precipitation data, a warning system or a prediction model may be accordingly created to prevent losses of lives and economic activities. Moreover, the scope or feasibility of the proposed model can be extended to other research fields so as to benefit human beings.

REFERENCES

[1] Central Weather Bureau. *Climate change report in Taiwan 1897-2008*. Taiwan: Ministry of Transportation and Communications, 2009.

[2] M. Muller, J. A. Tencate, T.W. Darling, A. Sutin, R.A. Guyer, M. Talmant, P. Laugier, and P.A. Johnson, "Bone micro-damage assessment using non-linear resonant ultrasound spectroscopy (NRUS) techniques: A feasibility study," *Ultrasonics*, vol. 44, pp. 245-249, 2006.

[3] M. J. Olsen, F. Kuester, B. J. Chang, and T. C. Hutchinson, "Terrestrial laser scanning-based structural damage assessment," *Journal of Computing in Civil Engineering*, vol. 24, pp. 264-272, 2010.

[4] M. –C. Su, D. –Y. Huang, J. –H. Chen, W. –Z. Lu, L. –C. Tsai, and J. –Z. Lin, "Mapping multi-spectral remote sensing images using rule extraction approach," *Expert Systems with Applications*, vol. 38, pp. 12917-12922, 2011.

[5] D. Brunner, G. Lemoine, and L. Bruzzone, "Earthquake damage assessment of buildings using VHR optical and SAR imagery," *IEEE Transactions on Geoscience and Remote Sensing*, vol. 48, pp. 2403-2420, 2010.

[6] G. Newaz, and X. Chen, "Progressive damage assessment in thermal barrier coatings using thermal wave imaging technique," *Surface and Coatings Technology*, vol. 190, pp. 7-14, 2005.

[7] D. W. Wilkinson, and M. K. Crosby, "Rapid assessment of forest damage from tornadoes in Mississipal," *Photogrammetric Engineering and Remote Sensing*, vol. 76, pp. 1299-1301, 2010.

[8] S. Voigt, T. Schneiderhan, A. Twele, M. Gähler, E. Stein, and H. Mehl, "Rapid damage assessment and situation mapping: Learning from the 2010 Haiti earthquake," *Photogrammetric Engineering and Remote Sensing*, vol. 77, pp. 923-931, 2010

[9] S. Stramondo, C. Bignami, M. Chini, N. Pierdicca, and A. Tertulliani, "Satellite radar and optical remote sensing for earthquake damage detection: Results from different case studies," *International Journal of Remote Sensing*, vol. 27, pp. 4433-4447, 2006.

[10] U. Cheema, "Expert systems for earthquake damage assessment," *IEEE Aerospace and Electronic Systems Magazine*, vol. 22, pp. 6-10, 2007.

[11] A., Kumar, R. K., Chingkhei, and T., Dolendro, "Tsunami damage assessment: A case study in Car Nicobar Island,"*India. International Journal of Remote Sensing*, vol.28, no.13-14, pp.2937-2959, 2007.

[12] C.-C., Liu, J.-G., Liu, C.-W., Lin, A.-M., Wu, S.-H., Liu, and C.-L., Shieh, "Image processing of FORMOSAT-2 data for monitoring the South Asia tsunami, " *International Journal of Remote Sensing*, vol.28, pp.3093-3111, 2007.

[13] F. Bovolo, and L. Bruzzone, "A split-based approach to unsupervised change detection in large-size multitemporal images: application to tsunami-damage assessment," *IEEE Transactions on Geoscience and Remote Sensing*, vol. 45, pp. 1658-1669, 2007.

[14] K. Dharanirajan, P. P. Kasinatha, B. Gurugnanam, R. M. Narayanan, and S. Ramachandran, "An integrated study for the assessment of tsunami impacts: A case study of South Andaman Island, India using remote sensing and GIS," *Coastal Engineering Journal*, vol. 49, pp. 229-266, 2007.

[15] P. Sirikulchayanon, W. Sun, and T. Oyana, "Assessing the impact of the 2004 tsunami on mangroves using remote sensing and GIS techniques," *International Journal of Remote Sensing*, vol. 29, pp. 3553-3576. 2008.

[16] A. M. Kerr, A. H. Baird, R. S. Bhalla, and V. Srinivas, "Reply to 'Using remote sensing to assess the protective role of coastal woody vegetation against tsunami waves," *International Journal of Remote Sensing*, vol. 30, pp. 3817-3820, 2009.

[17] K. Tsutsui, S. Rokugawa, H. Nakagawa, S. Miyazaki, C. -T. Cheng, T. Shiraishi, and S. -D. Yang, "Detection and volume estimation of large-scale landslides based on elevation-change analysis using DEMs extracted from high-resolution satellite stereo imagery," *IEEE Transactions on Geoscience and Remote Sensing*, vol. 45, pp. 1681-1696, 2007.

[18] M. -F. Lee, T. -C. Lin, M. A. Vadeboncoeur, and J. -L. Hwong, "Remote sensing assessment of forest damage in relation to the 1996 strong typhoon Herb at Lienhuachi Experimental Forest, Taiwan," *Forest Ecology and Management*, vol. 255, pp. 3297-3306, 2008.

[19] N. Silleos, K. Perakis, and G. Petsanis, "Assessment of crop damage using space remote sensing and GIS," *International Journal of Remote Sensing*, vol. 23, pp. 417-427, 2002.

[20] Y. Huang, S. J. Thomson, B.V. Ortiz, K.N. Reddy, W. Ding, R.M. Zablotowicz, and J. R. Bright, "Airborne remote sensing assessment of the damage to cotton caused by spray drift from aerially applied glyphosate through spray deposition measurements," *Biosystems Engineering*, vol. 107, pp. 212-220, 2010.

[21] S. Ekstrand, "Landsat TM-based forest damage assessment: Correction for topographic effects," *Photogrammetric Engineering and Remote Sensing*, vol. 62, pp. 151, 1996.

[22] A. S. Isaev, G.N. Korovin, S. A. Bartalev, D. V. Ershov, A. Janetos, E. S. Kasischke, H. H. Shugart, N. H. F. French, B. E. Orlick, and T.L. Murphy, "Using remote sensing to assess Russian forest fire carbon emissions," *Climatic Change*, vol. 55, pp. 235-249, 2002.

[23] C. Stone, R. Turner, and J. Verbesselt, "Integrating plantation health surveillance and wood resource inventory systems using remote sensing," *Australian Forestry*, vol. 71, pp. 245-253, 2008.

[24] T. M. Airola, "Monitoring the impact of arsenic contamination on forest vegetation in New Jersey using remote sensing techniques," *Journal of imaging technology*, vol. 16, pp. 120-123, 1990.

[25] F. Melgani, G. Moser, and S. B., Serpico, "Unsupervised change-detection methods for remote-sensing images," *Optical Engineering*, vol. 41, pp. 3288-3297, 2002.

[26] S. Kabir, P. Rivard, D. –C. He, and P. Thivierge, "Damage assessment for concrete structure using image processing techniques on acoustic borehole imagery," *Construction and Building Materials*, vol. 23, pp. 3166-3174, 2009.

[27] F. Wang, and Y. J., Xu, "Comparison of remote sensing change detection techniques for assessing hurricane damage to forests," *Environmental Monitoring and Assessment*, vol. 162, pp. 311-326, 2010.

[28] Z. Chen, and T. C., Hutchinson, "Probabilistic urban structural damage classification using bitemporal satellite images," *Earthquake Spectra*, vol. 26, pp. 87-109, 2010.

[29] K. Johansen, S. Phinn, J. Lowry, and M. Douglas, "Quantifying indicators of riparian condition in Australian tropical savannas: Integrating high spatial resolution imagery and field survey data," *International Journal of Remote Sensing*, vol. 29, pp. 7003-7028, 2008.

[30] T. M. Pavelsky, and L. C. Smith, "RivWidth: A software tool for the calculation of river widths from remotely sensed imagery," *IEEE Geoscience and Remote Sensing Letters*, vol. 5, pp. 70-73, 2008.

[31] Y. A. Liou, S. K. Kar, and L. Y. Chang, "Use of high-resolution FORMASAT-2 satellite images for post-earthquake disaster assessment: A student following 12 May 2008 Wenchuan earthquake," *International Journal of Remote Sensing*, vol. 31, pp. 3355-3368, 2010.

[32] J. –H. Chen, M. –C. Su, Y. –X. Zhao, Y. –J. Hsieh, and W. –H. Chen, "Application of SOMO based clustering in building renovation," *International Journal of Fuzzy Systems*, vol. 10, pp. 195-201, 2008.

[33] J. –H. Chen, M. –C. Su, and L. –R. Yang, "Comparison of SOM-based optimization and particle swarm optimization for minimizing the construction time of a secant pile wall," *Automation in Construction*, vol. 18, pp. 844-848, 2009.

[34] J. –H. Chen, M. –C. Su, and D. –Y. Huang, "Application of SOM-based optimization algorithm in minimizing construction time for secant pile wall," *Journal of Construction Engineering and Management*, vol. 136, pp. 1189-1195, 2010.

[35] Directorate General of Highways, *Disaster Assessment Report for Bridges Damaged by Typhoon Morakot*. Taipei, Taiwan: Ministry of Transportation and Communications, 2010.